Proton scattering from ^{154}Sm and ^{176}Yb at 0.8 GeV

M. L. Barlett, J. A. McGill, L. Ray, M. M. Barlett, and G. W. Hoffmann
Department of Physics, The University of Texas, Austin, Texas 78712

N. M. Hintz, G. S. Kyle,* and M. A. Franey
Department of Physics, University of Minnesota, Minneapolis, Minnesota 55455

G. Blanpied
Department of Physics, University of South Carolina, Columbia, South Carolina 29208
(Received 28 March 1980)

Elastic and inelastic angular distributions for 0.8 GeV p + ^{154}Sm and ^{176}Yb are reported and analyzed using the distorted-wave Born approximation and the coupled-channels formalism where phenomenological deformed optical potentials are used in the latter analysis. As expected, the multipole moments extracted from the optical potentials are found to be in excellent agreement with those of the charge densities as obtained from electron scattering and Coulomb excitation experiments. The analysis also clearly demonstrates that multistep processes are important at 0.8 GeV and must be included for a proper description of the experimental data.

[NUCLEAR REACTIONS ^{154}Sm(p,p'), ^{176}Yb(p,p'), $E=0.8$ GeV, measured $\sigma(\theta)$; enriched targets; resolution ~50 keV, $\theta_{c.m.}=4.5°$ to 21°, $\Delta\theta=0.1°$; optical model potential, DWBA analysis, coupled-channels analysis, rotational model, multipole moments.]

I. INTRODUCTION

One of the primary reasons for conducting intermediate energy (E_{inc} ~ 1 GeV) proton-nucleus scattering experiments is that accurate microscopic descriptions of the scattering process allow new nuclear structure information to be deduced through theoretical analyses of the data.[1] In particular, the connection between the underlying nuclear densities and the resulting optical potential for elastic and inelastic scattering, using nucleon-nucleon phenomenology, is fairly direct. As a result, a great deal of effort has been devoted recently to the determination of ground state matter density distributions for spherical nuclei through analyses of ~1 GeV proton elastic scattering data.[2-5] Similarly, the matter transition densities for a few spherical nuclei have been examined through microscopic analyses.[3,6-8] Generally, these efforts have shown that the matter and charge densities are quite similar, and the current effort is concentrated on accurately determining the relatively small differences between the two.[2-5]

In the present work we are led to the consideration of permanently deformed nuclei. The work presented here is aimed at determining whether or not the extracted deformed ground state matter density distribution is also similar to the deformed charge distribution. We report and analyze elastic and inelastic angular distribution data for 0.8 GeV proton scattering from ^{154}Sm and ^{176}Yb; these being two nuclei for which electron scattering and Coulomb excitation experiments have provided information about the deformed charge densities.[9-15] Specifically, we compare the first few multipole moments of the charge density with the approximately determined multipole moments of the matter distribution and then attempt to extract information about higher multipole moments from the 0.8 GeV proton data. Particular attention is given to the proper handling of multistep processes which have been shown to be important in 0.8 GeV proton inelastic excitation of states in ^{12}C and ^{24}Mg.[16,17] Studies of the full deformed matter distributions and the differences between the deformed proton and neutron distributions will be considered in future analyses.

In Sec. II the experimental techniques used to obtain the data are summarized. Some theoretical considerations and a description of the nuclear structure and reaction models assumed in the analysis are given in Sec. III. The results of the calculations and a comparison of the extracted and the charge density multipole moments are presented in Sec. IV. Finally, a summary and some conclusions are given in Sec. V.

II. EXPERIMENTAL

The data were obtained using the high resolution spectrometer (HRS) facility of the Los Alamos Clinton P. Anderson Meson Physics Facility (LAMPF). The HRS has been described else-

where.[18,19] The targets consisted of a 26.8 mg/cm^2 ^{176}Yb foil, enriched to 96.43% and a 29.2 mg/cm^2 ^{154}Sm foil enriched to 98.69%. The overall experimental energy resolution was typically 45–60 keV full width at half maximum (FWHM) for full HRS acceptance and was obtained by phase space control of the 800 MeV proton beam with five beam phase space collimators and through use of a multipole magnet located between the two HRS dipoles.[20]

A typical spectrum for ^{176}Yb is shown in Fig. 1. The data were obtained over the center of mass angular range 4°–20°. Angular distributions for excitation of the (0.0 MeV, 0_1^+), (0.082 MeV, 2_1^+), (0.272 MeV, 4_1^+), (0.565 MeV, 6_1^+), and (0.955 MeV, 8_1^+) states in ^{176}Yb and the (0.0 MeV, 0_1^+), (0.082 MeV, 2_1^+), (0.267 MeV, 4_1^+), and (0.544 MeV, 6_1^+) states in ^{154}Sm were extracted from the spectra and are shown in Figs. 2–9 together with theoretical curves to be discussed. In addition, angular distributions for the (0.903 MeV, 8_1^+)-(0.922 MeV, 1_1^-) unresolved doublet and the (1.013 MeV, 3_1^-) state in ^{154}Sm were also obtained and are shown in Fig. 7 along with theoretical predictions to be discussed. It was not possible to extend the angular distributions shown in Figs. 2–9 to more forward angles because of oxygen contamination of both targets.

A limited amount of $p+^{208}$Pb elastic angular distribution data was obtained during the course of the experiment and comparison with the data reported in Ref. 5 enabled absolute normalization and absolute scattering angle determinations of ±10% and ±0.1°, respectively, for the data reported here. The errors shown in Figs. 2–9 are statistical only.

III. THEORY

The theoretical description of nucleon-nucleus scattering at intermediate energies is generally

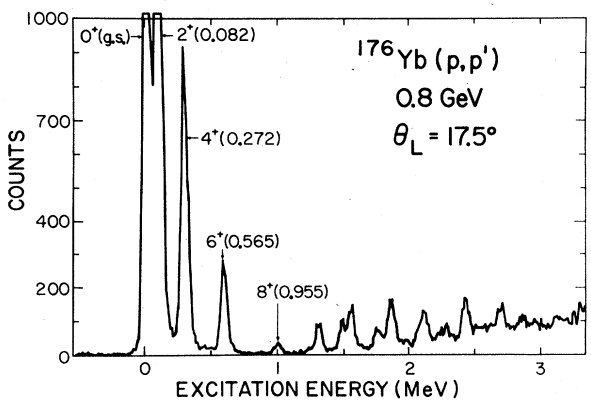

FIG. 1. A typical spectrum for 0.8 GeV $p+^{176}$Yb at $\theta_L = 17.5°$.

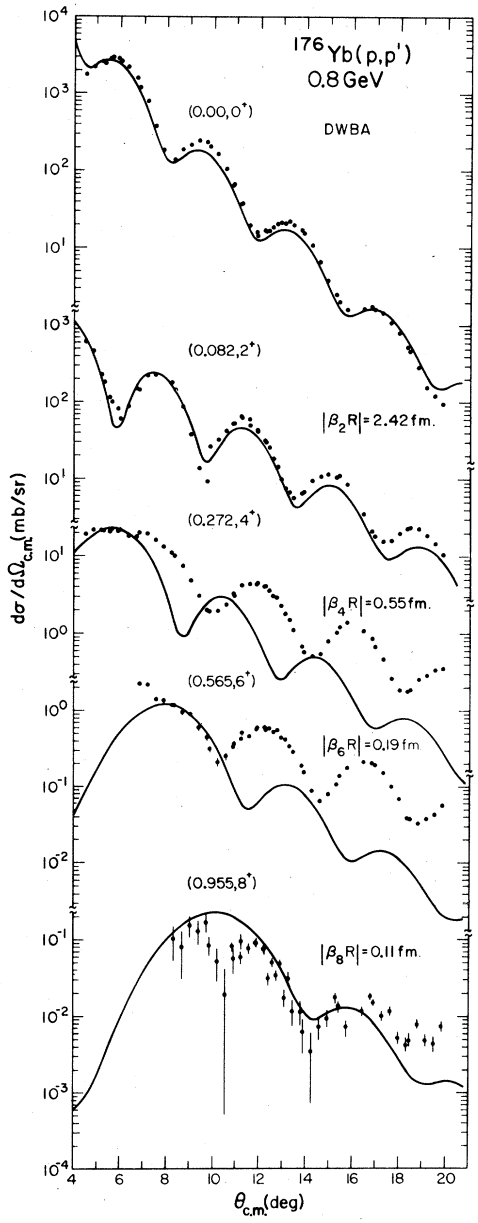

FIG. 2. Experimental angular distributions for ^{176}Yb (p,p') at 800 MeV and the results of DWBA calculations as discussed in the text.

given in the framework of the Kerman, McManus, and Thaler (KMT) optical potential formalism.[1] In the impulse approximation[1] the first order optical potential is obtained by folding the free nucleon-nucleon t matrix with the uncorrelated, one-body nuclear density. In coordinate space this lowest order optical potential is written as

$$V(\vec{r}) = \int \rho_m(\vec{r}\,')\tilde{t}(|\vec{r}-\vec{r}\,'|)d^3r' , \qquad (1)$$

where ρ_m is the point matter density distribution and $\tilde{t}$ is the averaged proton-nucleon free scatter-

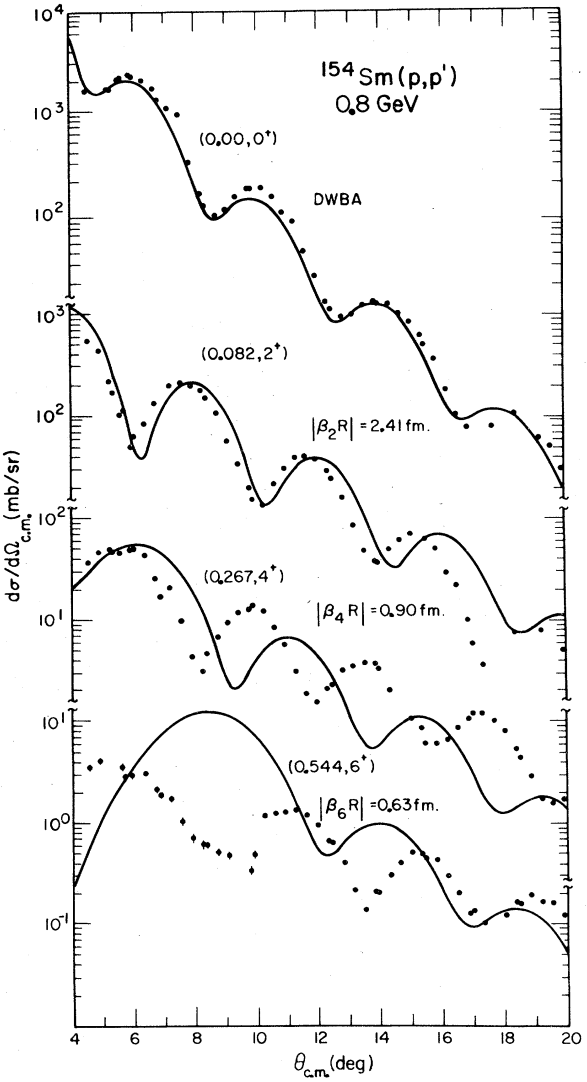

FIG. 3. Experimental angular distributions for ^{154}Sm (p,p') at 800 MeV and the results of DWBA calculations as discussed in the text.

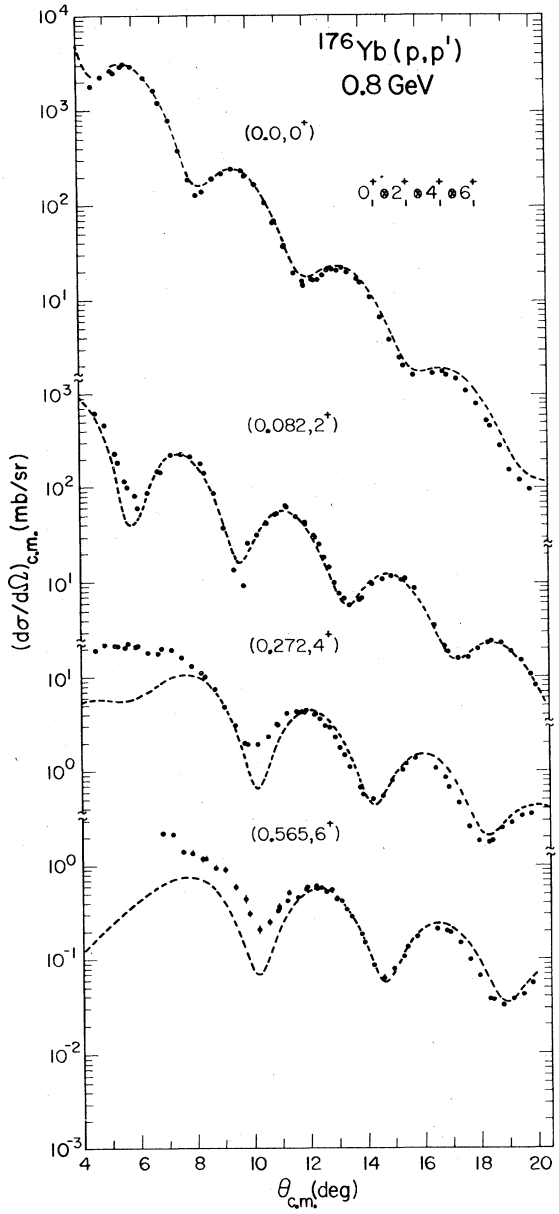

FIG. 4. Results of coupled channels calculations for ^{176}Yb using a deformed, axially symmetric rotational model, coupling the 0_1^+, 2_1^+, 4_1^+, and 6_1^+ states with the optical potential parameters of Table II.

ing amplitude.[1] Many examples can be found in the literature of applications of this folding model to ~1 GeV proton elastic and inelastic scattering from light deformed nuclei[18,19,21] and spherical nuclei.[2-7] The results indicate that folding models in general describe these ~1 GeV proton data extremely well. In fact, the lowest order KMT microscopic optical potential gives a very good description of these data, and corrections are rather small for nuclei with $A \geq 12$.[2,3] Density dependent and nonlocal effects which are present in principle are apparently not too important in practice.[1-3,22] Certainly more quantitative theoretical study is necessary before one can claim to completely understand the ~1 GeV proton-nucleus interaction at the microscopic level, but the work done to date clearly demonstrates the success of folding model descriptions of ~1 GeV proton-nucleus scattering. Therefore, in this paper we will assume that the ~1 GeV p+ heavy deformed nucleus optical potential can also be obtained in principle by folding a spherically symmetric proton-nucleon effective interaction with the deformed nuclear ground state density as in

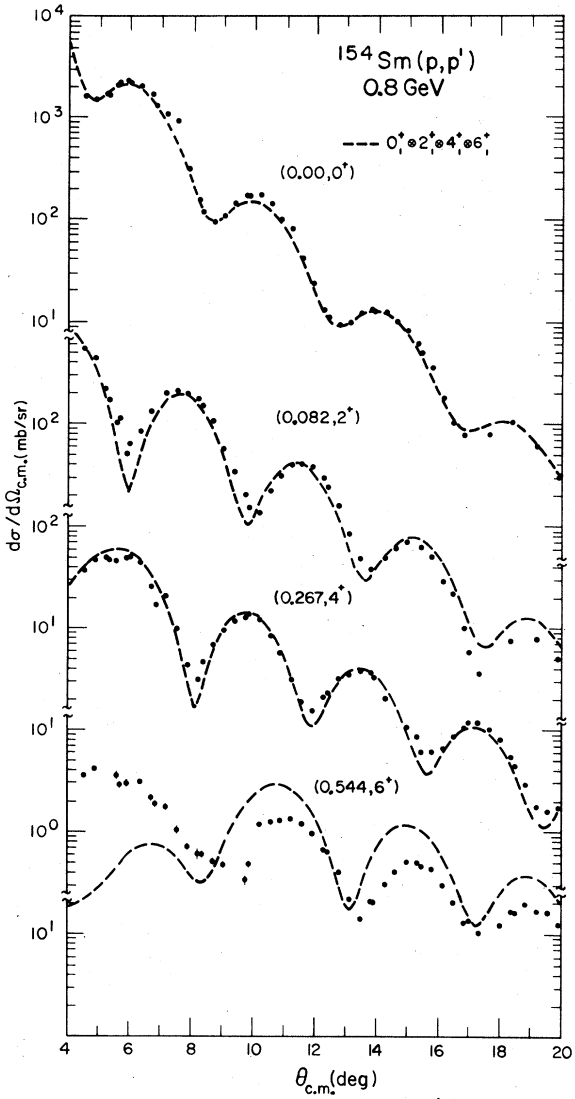

FIG. 5. Same as Fig. 4 except for ^{154}Sm.

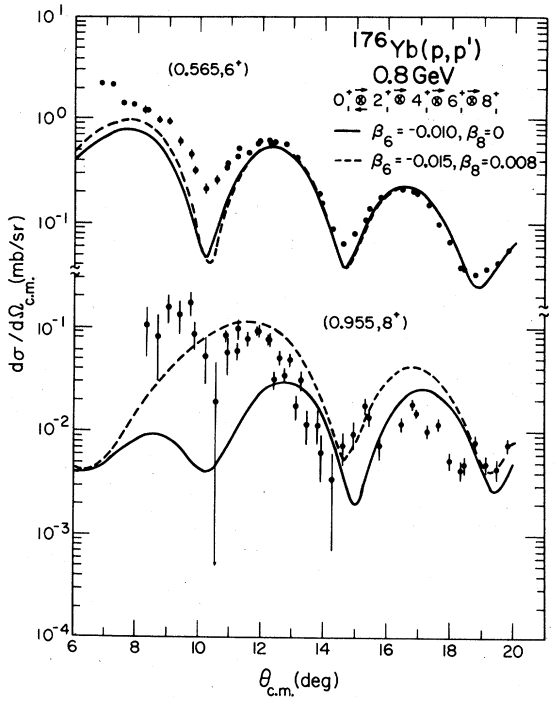

FIG. 6. Coupled channels calculations for the 6_1^+ and 8_1^+ transitions in ^{176}Yb. The symbol ⊛ indicates a full, two-way coupling as in all previous figures while the symbol ⊗ indicates an "excitation only" coupling as discussed in the text (see Sec. IV).

Eq. (1).

By fitting the elastic and inelastic scattering data for $p+^{154}$Sm and ^{176}Yb with multistep processes included, we will determine a deformed optical potential, $V(\vec{r})$. Then from the assumed applicability of the folding model, Eq. (1), and Satchler's theorem,[23] the multipole moments of the matter density[24] will be obtained from those of the optical potential. Satchler's theorem states that in units for which $\int \tilde{t} d^3r = 1$ the $(E\lambda)$ multipole moment of $V(\vec{r})$ in Eq. (1) is equal to the same $(E\lambda)$ moment of $\rho_m(\vec{r})$. The multipole moments of the optical potential, $V(r, \theta')$ (axially symmetric in the body fixed coordinate system[25]) quoted below are defined as [9,23]

$$M(E\lambda) = \frac{Ze \int r^\lambda Y_{\lambda 0}(\Omega') V(r, \theta') r^2 dr d\Omega'}{\int V(r, \theta') r^2 dr d\Omega'} . \qquad (2)$$

In Eq. (2), the charge of the target nucleus Ze is included to allow direct comparison between the optical potential quantities and the charge distribution moments. Thus, we expect the $M(E\lambda)$ moments of the empirical 0.8 GeV proton optical potential to be close to those of the matter densities of ^{154}Sm and ^{176}Yb. The extraction of $\rho_m(\vec{r})$ itself, not just the multipole moments, must await a better knowledge of the free nucleon-nucleon amplitudes at 800 MeV [Ref. (2)] and more exhaustive studies of corrections to the impulse approximation.[2,22]

It is appropriate to comment on the expected validity of similar results obtained through analysis of low energy nucleon- and composite particle-nucleus scattering data. Although microscopic descriptions of the low energy projectile-nucleus interaction for projectiles with $A \leq 4$ have improved remarkably in recent years,[26-29] they remain insufficiently accurate for careful determinations of matter density distributions. The effects of Pauli blocking,[26] exchange,[26,28] and the total momentum dependence of the proton-nucleon scattering amplitude[30] result in significant density dependence[26,28] and nonlocality corrections[30] which make it difficult to theoretically justify the use of the folding model for describing low energy, light

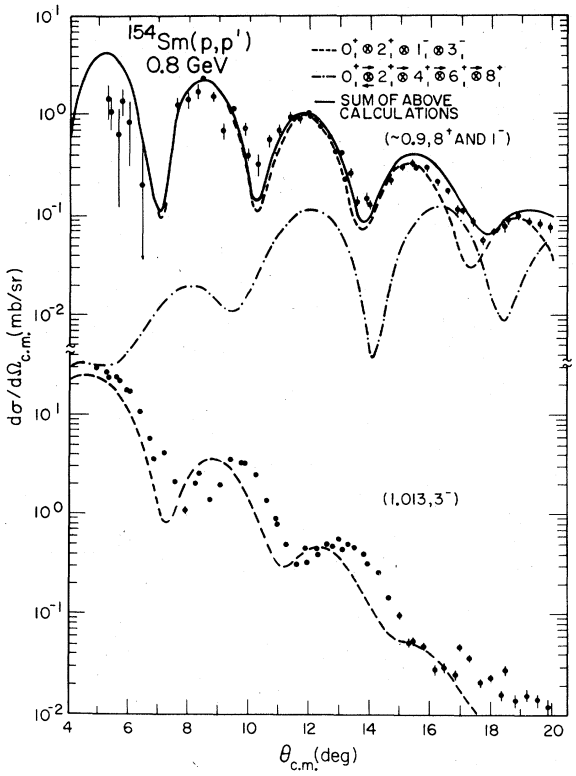

FIG. 7. Experimental angular distributions and coupled channels predictions for the $(8_1^+ - 1_1^-)$ doublet and the 3_1^- state in ^{154}Sm as discussed in the text. The coupling symbols are the same as in Fig. 6. The solid curve is the sum of the CC results for the 8_1^+ and the 1_1^- angular distributions.

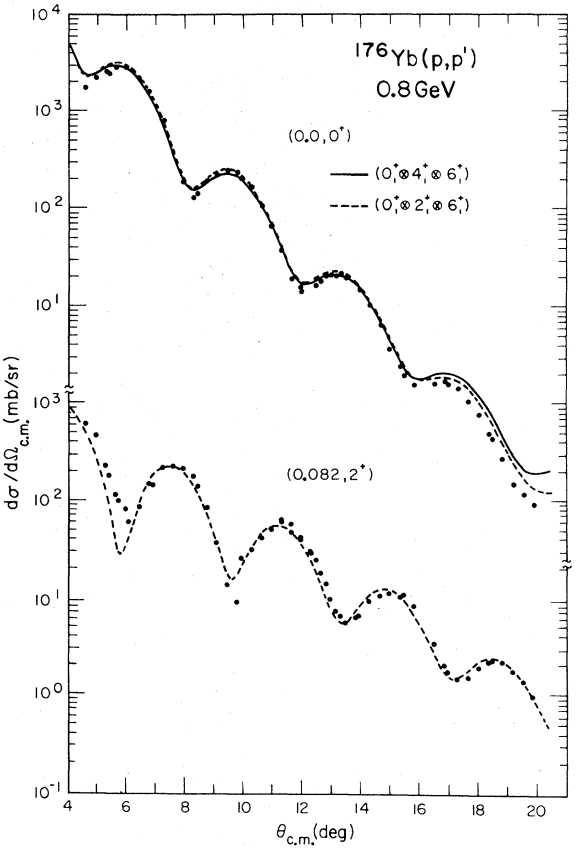

FIG. 8. Results of coupled channels calculations for ^{176}Yb(p,p') elastic and 2_1^+ transitions in which various coupling channels are omitted as discussed in the text.

ion scattering. These theoretical considerations cast doubt on the accuracy of even simple multipole moments determined through analysis of low-energy data. However, despite these theoretical drawbacks, if it can be demonstrated that a phenomenological folding model is capable of accurately describing a particular set of low energy scattering data, then at least the multipole moments of the matter densities can be obtained. For example, the success of folding model descriptions of $\gtrsim$100 MeV alpha scattering[31] data implies that the multipole moments of the underlying densities can be obtained from the folding potential.[32]

As stated previously, it is known that multistep processes must be carefully included for a proper theoretical description of ~1 GeV proton-nucleus inelastic scattering data for deformed nuclei. In order to gain a proper appreciation of the large deformation and multistep effects which contribute to the inelastic excitations reported here, in the next section we will give the results of simplified direct step calculations. For these calculations we assume that the deformed optical potential $V(\vec{r})$ can be expanded as[25]

$$V(\vec{r}) \cong V_0(r) - \sum_{\lambda\mu} \delta_\lambda \frac{d}{dr} V_0(r) D^\lambda_{\mu 0} Y_{\lambda\mu}(\theta, \phi)$$
$$\equiv V_0(r) + V_{\text{couple}}(\vec{r}) . \tag{3}$$

The coupling term V_{couple}, when evaluated in the nuclear matrix element, becomes

$$\langle IM | V_{\text{couple}} | 00 \rangle = - \frac{\delta_I}{(2I+1)^{1/2}} \frac{d}{dr} V_0(r) Y_{IM}(\theta, \phi) , \tag{4}$$

where $|00\rangle$ represents the ground state and $|IM\rangle$ the excited member of the ground state rotational band.[33] The above potential is used in the distorted-wave Born approximation (DWBA) [Ref. (34)] where the distorted waves are computed from $V_0(r)$ and only first order terms in δ_I contribute to the inelastic transition. Thus important multistep processes and second and higher order quadrupole deformation contributions to the inelastic transitions are neglected.

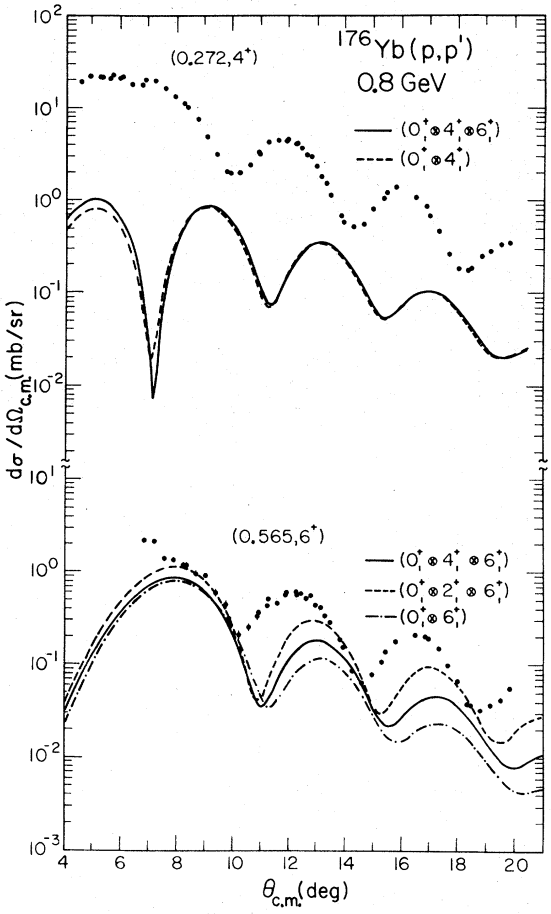

FIG. 9. Results of coupled channels calculations for ^{176}Yb(p,p') excitation of the 4^+_1 and 6^+_1 states with various intermediate coupling channels omitted as discussed in the text.

In order to include these effects, coupled-channels (CC) analyses of the 0^+_1, 2^+_1, 4^+_1, 6^+_1, and 8^+_1 transitions ($K^\pi = 0^+$) in ^{154}Sm and ^{176}Yb are then made, assuming the strict rotational model,[33] where the deformation of the potential shape is treated using the Legendre polynomial expansion method discussed by Tamura in Ref. 25, with axially symmetric deformations through β_8 allowed. The geometry of the optical potential is the usual Fermi form[25] where the radius parameter $R(\theta')$ is angle dependent, according to

$$R(\theta') = R_0\left[1 + \sum_{\lambda=2,\text{even}}^{8} \beta_\lambda Y_{\lambda 0}(\theta')\right]. \quad (5)$$

The 1^-_1 and 3^-_1 states of ^{154}Sm are assumed to be members of the $K^\pi = 0^-$ octupole-vibrational band[35,36] and are treated using the deformed-vibrational model.[37,38]

The spin-orbit potential is omitted from both the DWBA and coupled-channels calculations reported in Sec. IV for the following reasons. DWBA calculations for 0.8 GeV proton inelastic scattering to low lying, natural parity collective states have shown that equivalent predictions of inelastic angular distributions result when either spin-orbit terms are omitted or fully included (both in the diagonal and nondiagonal parts of the optical potential), provided equivalent fits to the elastic data are obtained.[39] Since the coupled-channels codes JUPITER[37] and CHORK[40] used in this analysis do not include provisions for spin-orbit deformation, and since the concern here is with angular distributions only, the spin-orbit potentials are omitted from both the diagonal and coupling potentials. The importance of deformed spin-orbit coupling in transitions which are dominated by multistep mechanisms is a refinement which one should consider in future analyses.[41]

IV. RESULTS OF THE ANALYSIS

A. DWBA calculations

The elastic angular distributions were fit using the optical model with relativistic kinematics[18] with a spherical Woods-Saxon potential $V_0(r)$ of Eq. (3). The potential parameters are given in Table I in the usual low energy notation.[42] The fits to the elastic angular distributions are shown in Figs. 2 and 3 as the solid curves.

The DWBA calculations were done using a version of the program VENUS[43] which was modified to include relativistic kinematics.[18] The optical potentials of Table I were used to generate the distorted waves and the standard derivative-like collective model form factors according to Eq. (4). The results for the 2^+_1, 4^+_1, 6^+_1, and 8^+_1 $p + ^{176}$Yb angular distributions are shown in Fig. 2 as the solid curves, while the 2^+_1, 4^+_1, and 6^+_1 results for ^{154}Sm are compared (solid curves) with the data in Fig. 3. The deformation lengths, $|\delta_l|$, are listed in Table I.

It is evident from Figs. 2 and 3 that only for the case of the 2^+_1 transitions does the DWBA produce reasonable fits to the angular distributions. For the 4^+_1 and 6^+_1 angular distributions the fits are poor, exhibiting incorrect angular positions of the diffractive maxima and minima, and too rapid a decrease between successive maxima. For the ^{176}Yb 4^+_1 transition the predicted diffractive structure in the angular distribution is shifted to smaller angles as compared to the data, while the opposite is true for the ^{154}Sm 4^+_1 case. This is due to the sign difference in the hexadecupole deformation of these nuclei and is discussed below. Although the prediction for the ^{176}Yb 8^+_1 angular distribution is in phase with the data, it also appears

TABLE I. Optical potential parameters and deformation lengths used in the DWBA calculations for ^{176}Yb and ^{154}Sm.

Nucleus	V (MeV)	W (MeV)	r (fm)	a (fm)	r_w (fm)	a_w (fm)	r_c (fm)
		Optical potential parameters					
^{176}Yb	−6.31	61.5	1.097	0.708	1.075	0.763	1.05
^{154}Sm	−5.35	59.5	1.077	0.864	1.075	0.712	1.05
		Deformation lengths (fm)					
		$\lvert\delta_2\rvert$	$\lvert\delta_4\rvert$		$\lvert\delta_6\rvert$	$\lvert\delta_8\rvert$	
	^{176}Yb	2.42	0.55		0.19	0.11	
	^{154}Sm	2.41	0.90		0.63		

to fall off too rapidly with increasing angle.

The failure of the DWBA to reproduce the angular distributions for transitions to the higher lying ground band states in both nuclei was also found in a similar study of 0.8 GeV $p + {}^{12}$C,^{24}Mg and was attributed to the neglect of multistep processes.[16,17] Since multistep processes are also expected to be important for 0.8 GeV $p + {}^{154}$Sm, ^{176}Yb, a coupled-channels analysis was done as discussed next.

B. Coupled-channels analysis, ground band rotational states through $I^\pi = 6_1^+$ in ^{154}Sm and ^{176}Yb

CC calculations for the 0_1^+, 2_1^+, 4_1^+, and 6_1^+ transitions ($K^\pi = 0^+$) in ^{154}Sm and ^{176}Yb were made using a modified version of the program JUPITER.[37] These modifications consisted of the inclusion of relativistic kinematics[18] and the incorporation of a larger number of allowable partial waves and mesh points for use with heavy nuclei at intermediate energies. All possible couplings between the 0_1^+, 2_1^+, 4_1^+, and 6_1^+ channels through $\Delta l = 8$ were assumed in the analysis. Higher angular momentum couplings were not included due to code limitations. The truncation of coupling potential terms with $\Delta l > I_{\max}$ ($I_{\max}$ being the largest value of total angular momentum of the coupled states) has been shown to have negligible effects on the predicted 4_1^+ and 6_1^+ angular distributions. Therefore the coupling terms with $\Delta l > 8$ are not expected to contribute significantly to the 6_1^+ or 8_1^+ transitions. The optical potentials and deformation parameters were adjusted to simultaneously optimize the fits to the angular distributions of the 0_1^+, 2_1^+, 4_1^+, and 6_1^+ states with priority being given to the lower lying states.

The results of the CC calculations for ^{176}Yb and ^{154}Sm are shown in Figs. 4 and 5, respectively. The parameters of the deformed optical potentials for both nuclei are given in Table II. Also found in Table II is an alternate set of optical potential parameters for ^{154}Sm which give equivalent fits to the 0_1^+, 2_1^+, and 4_1^+ angular distributions, thus indicating some ambiguity in the empirical determination of the optical potential. The same deformation parameters were used for the two sets of optical potentials. The diagonal parts of the

TABLE II. Deformed optical potential parameters used in the coupled-channels calculations for ^{176}Yb and ^{154}Sm.

Nucleus	V (MeV)	W (MeV)	r (fm)	a (fm)	r_w (fm)	a_w (fm)	r_c (fm)
		Optical potential parameters					
^{176}Yb	−6.31	85.0	1.097	0.708	1.060	0.630	1.05
^{154}Sm	−5.35	59.5	1.077	0.846	1.113	0.575	1.05
^{154}Sm (alt. set)	−5.35	70.0	1.077	0.846	1.075	0.600	1.05
		Deformation parameters					
		β_2	β_4		β_6	β_8	
	^{176}Yb	0.330	−0.045		−0.010	0.0	
	^{176}Yb	0.330	−0.045		−0.015	0.008	
	^{154}Sm	0.301	0.110		−0.016	0.0	

two optical potentials for ^{154}Sm differ by 10.5 MeV at the center of the nucleus but gradually converge and become indistinguishable beyond about 6 fm, the approximate half-potential radius. This provides further indication of the region of the nuclear potential to which 0.8 GeV protons are most sensitive.[2] However, as discussed below, the lack of variation in the deduced multipole moments of these two potentials indicates the relative unimportance of optical model ambiguities in their determination.

As seen in Fig. 4, the angular distributions for transitions to the ground state rotational band of ^{176}Yb (through the 6_1^+ transitions) are adequately reproduced by the CC predictions. The deviation between the predictions and the data at forward angles for the 4_1^+ and 6_1^+ states is presently under investigation.

The same conclusions are drawn concerning the ^{154}Sm angular distribution (Fig. 5), except that for the 6_1^+ case the calculation is slightly out of phase with the data and the predicted magnitudes are about a factor of 2 larger than the data. No reasonable variation in β_6 or β_8 was able to eliminate this discrepancy. Similar discrepancies between data and CC calculations without the spin-orbit potential were seen in the analysis of 35 MeV proton scattering from ^{154}Sm reported in Ref. 41; a CC calculation with the full spin-orbit potential included showed a significant change in the overall slope and the angular positions of the maxima and minima of the predicted 6_1^+ angular distribution. The effects of including the spin-orbit potential in the CC analyses of higher lying collective states excited by 0.8 GeV protons will be the subject of future investigation. Such an effort is also motivated by the fact that CC calculations describe alpha inelastic excitation of the 6_1^+ state very well.[44]

It is possible that the higher spin states in ^{154}Sm are not adequately described using the strict rotational model, and this could account for the discrepancy seen in the 6_1^+ angular distribution. However, an examination of empirical and rotational model values of $B(E2)$ was made, and no significant difference was found here and in Ref. 45 between these quantities, suggesting that ^{154}Sm is adequately represented by the rigid rotator, at least with respect to $B(E2)$ values.

The extracted multipole moments, [Eq. (2)] of the dominant imaginary (best determined) part of the 800 MeV optical potential are given in Table III, along with those obtained in similar analyses of low energy proton,[41,46-49] alpha,[44,50] and electron[14,15] inelastic scattering data and from Coulomb excitation measurements.[9-13] Some theoretical predictions are also given.[15,51,52]

Table III indicates that the moments determined in this analysis agree remarkably well with those of the charge densities and suggests that the deformations of the proton and neutron distributions are nearly equal in these two nuclei. This is predicted by the density-dependent Hartree-Fock calculations of Negele and Rinker.[41,52] Also given in Table III are the percentage differences between our results for $M(E2)$ values and other reported values. The difference between our results and the electromagnetic values is typically 1–2%, while the low energy proton and alpha analyses yield values that are quite scattered and differ by a few to 20%. Good agreement between our $M(E4)$ and the charge density values is also seen, especially for ^{154}Sm, whereas wide scatter is found in the published values obtained from low energy efforts as was the case with $M(E2)$. Thus, analysis of 800 MeV p + nucleus inelastic scattering data appears to be a more accurate method for studying deformed matter distributions in nuclei than analysis of low energy scattering data, even with respect to the lowest $M(E2)$ multipole moment.

The alternate optical potential in Table II for ^{154}Sm yields multipole moments $M(E2)$, $M(E4)$, and $M(E6)$ which are, respectively, 6%, 12%, and 16% smaller than the first ^{154}Sm optical potential moments given in Table III. While this does not constitute a complete error analysis, it does provide some indication of the uncertainty in the extracted multipole moments due to optical model ambiguities.

C. Higher lying states in ^{154}Sm and ^{176}Yb

Coupled-channels predictions for the 8_1^+ angular distributions (^{176}Yb and ^{154}Sm) were obtained using the program CHORK,[40] which includes relativistic kinematics. Due to code limitations a number of simplifications were required in order to permit coupling through the 8_1^+ state. These simplifications included: (1) the assumption that the off-diagonal coupling potentials were imaginary, (2) the use of "excitation only" couplings; although multistep flux from the 2_1^+ channel back into the 0_1^+ channel was included, and (3) omission of all coupling potentials with $\Delta l > 8$. The optical potential parameters used were those given in Table II. The "excitation only" coupling means that the coupling of states $|I\rangle$ and $|I'\rangle$ appears as a source term in the $|I'\rangle$ channel for $I' > I$, but no inverse $|I'\rangle$ coupled to $|I\rangle$ "deexcitation" term appears in the $|I\rangle$ channel.[25] The calculations using these various truncations reproduced the 0_1^+, 2_1^+, 4_1^+ and 6_1^+ angular distributions quite well, so that the 8_1^+ predictions are considered reliable.

Results of the calculations described above are shown for the 8_1^+ state in ^{176}Yb in Fig. 6. Deforma-

TABLE III. Optical potential and charge density multipole moments in $eb^{\lambda/2}$.[a]

Nucleus	$M(E2)$	$M(E4)$	$M(E6)$	$M(E8)$	$\Delta(\%)$[b]	Reaction	E(MeV)	Reference
^{154}Sm	2.25	0.48			6	(p,p')	12	46
	1.95	0.43			−8	(p,p')	16	47
	2.06(3)	0.54(2)			−3	(p,p')	35	41
	2.10				−1	(p,p')	51	48
	2.54	0.73	0.064		20	(α,α')	35	50
	2.38	0.61	0.037		12	(α,α')	50	44
	2.12	0.58	0.099			(p,p')	800	This work
	2.076(6)	0.563(37)			−2	Coul. ex.		9,10[c]
	2.063(15)	0.58(14)			−3	Coul. ex.		11
	2.119(5)	0.631(48)			0	Coul. ex.		12
	|2.10| (2)	|0.470| (11)			−1	(e,e')[d]	35–110	14
	2.14	0.429			1	Theory		11,51
	1.98	0.43			−7	Theory[e]		41,52
^{176}Yb	2.65				15	(p,p')	16	49
	2.29(5)	−0.09(3)			−1	(p,p')	35	41
	2.94	−0.04			27	(α,α')	35	50
	2.76	−0.17	−0.15		19	(α,α')	50	44
	2.31	0.036	−0.048			(p,p')	800	This work
	2.31	0.029	−0.053	−0.0009		(p,p')	800	This work
	2.325(18)	$0.28^{+0.11}_{-0.20}$			1	Coul. ex.		13
	|2.30|	|0.0128|	|0.0538|		0	(e,e')[d]	50–320	15
	|2.35|	|0.078|	|0.092|		2	(e,e')[f]	50–320	15
	|2.43|	|0.074|	|0.065|		5	Theory		15
	2.47	0.052			7	Theory[e]		41,52

[a] Multipole moments are for the imaginary part of the optical potential for the present, 800 MeV work; the real part is used for all other hadronic scattering potentials. Volumes are normalized to Ze. For the 800 MeV ^{154}Sm moments the first optical potential set of Table II was used.

[b] $\Delta \equiv \{[M(E2) - M(E2 \text{ at } 800 \text{ MeV})]/M(E2 \text{ at } 800 \text{ MeV})\} \times 100\%$.

[c] The average of several Coulomb excitation measurements are quoted here.

[d] Fixed set of deformation parameters for all transitions.

[e] Proton and neutron moments are isospin averaged.

[f] Deformation parameters allowed to vary for each transition.

tion parameters for the solid curve are the same as those given in Table II with $\beta_8 = 0$, while the dashed curve was obtained using the same β_2 and β_4 of Table II, but $\beta_6 = -0.015$ and $\beta_8 = 0.008$. The use of the small, positive β_8 deformation in the calculation reproduced the magnitude and general shape of the 8_1^+ angular distribution but required the adjustment of β_6 in order to recover the fit to the 6_1^+ data. The predicted angular distributions for transitions to the lower-lying ground band states were unaffected by these adjustments to β_6 and β_8.

A similar calculation was made for the 8_1^+ transition in ^{154}Sm, using the parameters of Table II with $\beta_8 = 0$, in order to estimate the contribution of the 8_1^+ transition to the $(8_1^+ - 1_1^-)$ doublet angular distribution. The result is shown in Fig. 7 as the dash-dot curve. A value of β_8 large enough to reproduce the magnitude of the summed $(8_1^+ - 1_1^-)$ experimental cross section results in an angular distribution which is similar to the DWBA prediction of Fig. 2, and is therefore inconsistent with the data.

A CC calculation using **JUPITER** was also made for the ^{154}Sm 1_1^- and 3_1^- angular distributions. For these calculations the states were assumed to be members of the $K^\pi = 0^-$ octupole-vibrational band. The 0_1^+, 2_1^+, 1_1^-, and 3_1^- states were coupled using the same potential and deformation parameters as given in Table II, (β_6 was omitted, however, due to code restrictions for this deformed-vibrational case). The Y_{30} coupling length[37,38] of the ground band and the $K^\pi = 0^-$ vibrational band was found to be 0.38 fm by fitting the magnitude of the 3_1^- experimental cross section. The $K^\pi = 0^-$ vibrational strength was determined by normalizing to the 3_1^- cross section, since the contribution of the 1_1^- state to the $(8_1^+ - 1_1^-)$ experimental doublet is uncertain. The results of the calculations are indicated by the dashed curves in Fig. 7. The predicted 1_1^- angular distribution is correct in magnitude but slightly out-of-phase with the data at the back angles. The 3_1^- angular distribution, which was normalized to yield the correct magni-

tude, displays incorrect angular positions of the maxima and minima even at the first minimum. A calculation in which the 0_1^+, 2_1^+, 4_1^+, 1_1^-, and 3_1^- states were coupled produced no improvement in the predicted 3_1^- angular distribution. The omission of couplings to higher lying states in the $K^\pi = 0^-$ vibrational band or to other vibrational bands[36] might account for the angular shift between the calculated and experimental angular distributions for the 3_1^- transition. Other $K^\pi = 0^-$ vibrational multipoles might also be needed to resolve this discrepancy.[38]

Finally, the sum of the 8_1^+ and 1_1^- calculations is shown as the solid curve in Fig. 7. Good agreement with the data is now seen at the larger angles where phase differences occurred between the data and the CC calculation for the 1_1^- state. Apparently the 1_1^- transition provides the dominant strength, while the 8_1^+ angular distribution seems to provide sufficient strength at back angles to cause a correct shift in the position of the last minimum of the calculated angular distribution.

D. Importance of multistep processes

In order to demonstrate the effects of multistep processes in populating the higher lying states of the ground state rotational band in deformed rare earth nuclei, CC calculations were performed in which various couplings were selectively omitted for the 4_1^+ and 6_1^+ angular distributions for ^{176}Yb. Some of the results are shown in Figs. 8 and 9. Figure 8 shows that a good description of the elastic angular distribution can be obtained when either the 2_1^+ (solid curve) or the 4_1^+ (dashed curve) state is omitted from the coupling scheme. This figure also shows that omission of the 4_1^+ transition does not result in a poorer fit to the 2_1^+ angular distribution (see Fig. 4). It was necessary, however, to adjust the optical potential when the 2_1^+ state was removed from the coupling scheme in order to recover the fit to the elastic angular distribution. The resulting potential was varied relative to the initial parameter values listed in Table II in the following manner: W was decreased 3.6%, r_w was decreased 3.8%, and a_w was increased 12.7%. Thus, omitting the 2_1^+ channel resulted in a 17% *decrease* in the magnitude of the diagonal part of the imaginary optical potential at the half-potential radius 5.9 fm. Such effects are generally seen at intermediate energies where the optical potential is primarily imaginary.[16,17,53] Omitting the 4_1^+ and/or the 6_1^+ channels from the coupling scheme does not require a change of the optical potential parameters of Table II.

The calculated angular distribution for the 4_1^+ transition when the 2_1^+ channel was omitted, after recovery of the fit to the elastic angular distribution, is shown as the solid curve at the top of Fig. 9. The further omission of the 6_1^+ channel leads to the dashed curve in the upper portion of Fig. 9. These calculations indicate that the 4_1^+ state in ^{176}Yb is populated predominantly via a multistep process through the 2_1^+ channel. The direct step population of the 4_1^+ state and multistep population through the higher 6_1^+ state are less important. Figure 9 also demonstrates (lower half) the effects of omitting the intermediate 2_1^+ channel (solid curve), 4_1^+ channel (dashed curve), and both the 2_1^+ and 4_1^+ channels (dash-dot curve) on the predicted angular distribution for the 6_1^+ transition. It is clear that multistep processes play a significant role in the population of the 6_1^+ state and become increasingly important as momentum transfer increases. The calculations show that the most prominent intermediate channel in the population of the 6_1^+ state is the 2_1^+, as was the case for the 4_1^+ state, but that the 4_1^+ intermediate channel is also significant.

The main difference between the DWBA predictions made here according to Sec. III (Fig. 2) and the CC predictions shown in Fig. 9, which do not include intermediate state coupling, is that in the latter the Legendre polynomial expansion of the deformed optical potential is used, while in the former only the "direct" $\delta_l Y_l$ coupling term of the expansion is used [see Eq. (4)]. Thus, for example, in the CC calculation indicated by the dashed curve in Fig. 9 the 4_1^+ channel is reached directly via the $\delta_4 Y_4$ term, the $(\delta_2 Y_2)^2$ term, etc. Although the "coupling-omitted" curves shown in Fig. 9 are qualitatively more similar to the data than are the corresponding DWBA curves of Fig. 2, it is clearly evident (see Fig. 4) that multistep processes must be included in order to correctly predict the magnitude and angular structure of the experimental data.

As seen from the results shown in Fig. 9, the 800 MeV proton inelastic excitation of the 4_1^+ and 6_1^+ states in ^{176}Yb is almost entirely due to multistep processes. Multistep effects are also expected to be important in ~1 GeV proton inelastic excitation of the higher ground band states in other, similarly deformed rare earth nuclei.

V. SUMMARY AND CONCLUSIONS

New elastic and inelastic data for 0.8 GeV p + ^{176}Yb, ^{154}Sm have been presented and analyzed using the DWBA and CC formalisms. The DWBA calculations in general did not reproduce the experimental results, while transitions to members of the ground state rotational bands in both nuclei (except the 6_1^+ ^{154}Sm angular distribution) were

adequately described using the CC approach and the axially symmetric rotational model. Angular distributions for transitions to the 1_1^- and 3_1^- members of the $K^\pi = 0^-$ octupole-vibrational band in ^{154}Sm were analyzed using the deformed-vibrational model and CC techniques. The failure of the CC calculations for the 6_1^+ transition in ^{154}Sm, and the results of a study of deformed spin-orbit effects for the excitation of this state with 35 MeV protons, suggest that a similar study is warranted at 800 MeV.

The applicability of the folding model to ~1 GeV proton-nucleus scattering, together with Satchler's theorem, suggest that the multipole moments of the ~1 GeV proton-nucleus optical potential and those of the underlying matter density are nearly equal; excellent agreement between the multipole moments of the optical potential and the moments of the charge distributions in ^{154}Sm and ^{176}Yb was obtained. Considerable scatter in the multipole moments of the real parts of the low energy proton and alpha particle optical potentials is observed for these nuclei, where the simple folding model is certainly suspect from theoretical considerations.[26-29]

An investigation of the importance of multistep processes for 800 MeV proton excitation of the 4_1^+ and 6_1^+ states in ^{176}Yb was also carried out. The multistep mechanism was found to dominate the population of these higher spin states, with the 2_1^+ being the predominant intermediate channel. The 4_1^+ intermediate channel was also found to be important in the excitation of the 6_1^+ state.

Finally, the excellent fits obtained to the 800 MeV angular distributions, as well as the excellent agreement between the multipole moments obtained here and those of the charge densities, indicate that similar studies using other heavy deformed nuclei may provide more accurate determinations of the ground state matter deformations than can be obtained from lower energy work. Continued comparison of the multipole moments of ~1 GeV proton-nucleus optical potentials with charge density moments is clearly called for in order to further test the utility of intermediate energy protons as accurate probes of deformed ground state and transition matter densities. The present study also suggests that intermediate energy proton inelastic scattering may provide the best measurements of high multipoles ($\lambda > 4$) of the nucleus. These data should also prove useful in future studies of deformed nuclear matter distributions and in tests of microscopic descriptions of collective states.

This work was supported in part by the U.S. Department of Energy and the Robert A. Welch Foundation.

---

*Present address: SIN, 5234 Villigen, Switzerland.

[1]A. K. Kerman, H. McManus, and R. M. Thaler, Ann. Phys. (N.Y.) 8, 551 (1959).
[2]L. Ray, W. R. Coker, and G. W. Hoffmann, Phys. Rev. C 18, 2641 (1978); L. Ray, Phys. Rev. C 19, 1855 (1979).
[3]A. Chaumeaux, V. Layly, and R. Schaeffer, Ann. Phys. (N.Y.) 116, 247 (1978).
[4]G. Varma and L. Zamick, Phys. Rev. C 16, 308 (1977).
[5]G. W. Hoffmann *et al.*, Phys. Rev. C 21, 1488 (1980).
[6]G. S. Adams *et al.*, Phys. Rev. Lett. 43, 421 (1979).
[7]G. S. Adams *et al.*, Phys. Rev. C 21, 2485 (1980).
[8]Y. Abgrall, J. Labarsouque, B. Morand, and E. Caurier, Nucl. Phys. A316, 389 (1979).
[9]R. M. Ronningen *et al.*, Phys. Rev. C 16, 2208 (1977).
[10]A. H. Shaw and J. S. Greenberg, Phys. Rev. C 10, 263 (1974); F. S. Stephens, R. M. Diamond, and J. de Boer, Phys. Rev. Lett. 27, 1151 (1971); T. K. Saylor, J. X. Saladin, I. Y. Lee, and K. A. Erb, Phys. Lett. 42B, 51 (1972); W. Brückner *et al.*, Nucl. Phys. A231, 159 (1974); H. J. Wollersheim, W. Wilcke, T. W. Elze, and D. Pelte, Phys. Lett. 48B, 323 (1974); C. E. Bemis *et al.*, Phys. Rev. C 8, 1934 (1973).
[11]I. Y. Lee *et al.*, Phys. Rev. C 12, 1483 (1975).
[12]H. Fischer *et al.*, Phys. Rev. C 15, 921 (1977).
[13]H. J. Wollersheim, W. Wilcke, and T. W. Elze, Phys. Rev. C 11, 2008 (1975).
[14]T. Cooper *et al.*, Phys. Rev. C 13, 1083 (1976).
[15]C. W. Creswell, Ph.D. thesis, Massachusetts Institute of Technology, 1977 (unpublished).
[16]L. Ray, G. S. Blanpied, W. R. Coker, R. P. Liljestrand, and G. W. Hoffmann, Phys. Rev. Lett. 40, 1547 (1978).
[17]G. Blanpied *et al.*, Phys. Rev. C 20, 1490 (1979).
[18]G. S. Blanpied *et al.*, Phys. Rev. C 18, 1436 (1978).
[19]G. S. Blanpied *et al.*, Phys. Rev. Lett. 39, 1447 (1977).
[20]G. Blanpied, R. Liljestrand, G. W. Hoffmann, and J. E. Spencer, Nucl. Instrum. Methods 134, 421 (1976).
[21]C. Gustafsson and E. Lambert, Ann. Phys. (N.Y.) 111, 304 (1978).
[22]L. Ray, Phys. Rev. C 20, 1857 (1979).
[23]G. R. Satchler, J. Math. Phys. 13, 1118 (1972).
[24]D. M. Brink and G. R. Satchler, *Angular Momentum* (Oxford University Press, Oxford, 1968).
[25]T. Tamura, Rev. Mod. Phys. 37, 679 (1965); T. Tamura, Annu. Rev. Nucl. Sci. 19, 99 (1969).
[26]F. A. Brieva and J. R. Rook, Nucl. Phys. A291, 299 (1977); A291, 317 (1977).
[27]J. P. Jeukenne, A. Lejeune, and C. Mahaux, Phys. Rev. C 16, 80 (1977).
[28]B. Sinha, Phys. Rep. 20, 1 (1975).
[29]M. LeMere and Y. C. Tang, Phys. Rev. C 20, 2003 (1979).
[30]B. Mulligan, Ann. Phys. (N.Y.) 26, 159 (1964).
[31]G. M. Lerner, J. C. Hiebert, L. L. Rutledge, Jr.,

and A. M. Bernstein, Phys. Rev. C 6, 1254 (1972).
[32]A. M. Bernstein, *Advances in Nuclear Physics*, edited by M. Baranger and E. Vogt (Plenum, New York, 1969), Vol. 3, p. 325.
[33]A. Bohr and B. R. Mottelson, *Nuclear Structure*, Vol. II (Benjamin, Reading, Mass., 1975).
[34]G. R. Satchler, Nucl. Phys. 55, 1 (1964).
[35]E. Veje, B. Elbek, B. Herskind, and M. C. Olesen, Nucl. Phys. A109, 489 (1968).
[36]B. Harmatz, Nucl. Data Sheets 26, 281 (1979).
[37]T. Tamura, Oak Ridge National Laboratory Report No. ORNL-4152, 1967 (unpublished).
[38]L. Ray, G. S. Blanpied, and W. R. Coker, Phys. Rev. C 20, 1236 (1979).
[39]L. Ray and W. R. Coker, Phys. Lett. 79B, 182 (1978).
[40]Coupled-channels program of P. D. Kunz and modified by L. D. Rickertsen (unpublished).
[41]C. H. King, J. E. Finck, G. M. Crawley, J. A. Nolan, Jr., and R. M. Ronningen, Phys. Rev. C 20, 2084 (1979).
[42]C. M. Perey and F. G. Perey, Atomic Data Nucl. Data Tables 13, 293 (1974).
[43]T. Tamura, W. R. Coker, and F. Rybicki, Computer Phys. Commun. 2, 94 (1971).
[44]D. L. Hendrie *et al.*, Phys. Lett. 26B, 127 (1968).
[45]I. A. Fraser, J. S. Greenberg, S. H. Sie, R. G. Stokstad, and D. A. Bromley, Phys. Rev. Lett. 23, 1051 (1969).
[46]A. B. Kurepin, H. Schulz, and H. J. Wiebicke, Nucl. Phys. A189, 257 (1972).
[47]P. H. Brown and P. Stoler, Phys. Rev. C 2, 765 (1970).
[48]P. B. Woollam *et al.*, Nucl. Phys. A179, 657 (1972).
[49]T. Kruse *et al.*, Nucl. Phys. A169, 177 (1971).
[50]A. A. Aponick, Jr., C. M. Chesterfield, D. A. Bromley, and N. K. Glendenning, Nucl. Phys. A159, 367 (1970).
[51]U. Götz, H. C. Pauli, K. Alder, and K. Junker, Nucl. Phys. A192, 1 (1972).
[52]J. W. Negele and G. Rinker, Phys. Rev. C 15, 1499 (1977).
[53]L. Ray *et al.*, Phys. Lett. 83B, 275 (1979).